Published in final edited form as:
J Neuropathol Exp Neurol. 2012 November ; 71(11): 948–958. doi:10.1097/NEN.0b013e31826eaee7.

Exacerbation of Experimental Autoimmune Encephalomyelitis in the Absence of Breast Regression Protein-39/Chitinase 3-like-1

Dafna Bonneh-Barkay, PhD, **Guoji Wang, MS**, **William A. LaFramboise, PhD**, **Clayton A. Wiley, MD, PhD**, and **Stephanie J. Bissel, PhD**
Department of Pathology, University of Pittsburgh School of Medicine, Pittsburgh, Pennsylvania

Abstract

We previously reported that YKL-40, the human analog of mouse breast regression protein-39 (BRP-39; chitinase 3-like 1), is elevated in the cerebrospinal fluid of patients with a variety of neuroinflammatory conditions, such as multiple sclerosis and traumatic brain injury. YKL-40 expression in the CNS was predominantly associated with reactive astrocytes in the vicinity of inflammatory lesions. Because previous studies have shown that reactive astrocytes play a critical role in limiting immune infiltration in the mouse model of experimental autoimmune encephalomyelitis (EAE), we explored the role of BRP-39 in regulating neuroinflammation in EAE. Using BRP-39-deficient mice (BRP-39$^{-/-}$), we demonstrate the importance of BRP-39 in modulating the severity of clinical EAE and CNS neuroinflammation. At disease onset, absence of BRP-39 had little effect on clinical disease or lymphocytic infiltrate, but by 14 days post-immunization (dpi), differences in clinical scores were evident. By 28 dpi, BRP-39$^{-/-}$ mice showed more severe and persistent clinical disease than BRP-39$^{+/+}$ controls. Histopathological evaluation showed that BRP-39$^{-/-}$ mice had more marked lymphocytic and macrophage infiltrates and gliosis vs. BRP-39$^{+/+}$ mice. These findings support the role of BRP-39 expression in limiting immune cell infiltration into the CNS and offer a new target to modulate neuroinflammation.

Keywords

BRP-39; Chitinase-like proteins; Experimental autoimmune encephalomyelitis; Multiple sclerosis; Neuroimmunology; YKL-40

INTRODUCTION

Abundant expression of mammalian chitinases in general, and YKL-40 in particular, is observed in solid cancers and a variety of inflammatory diseases, including Crohn's disease, rheumatoid arthritis, osteoarthritis, and cirrhosis (1). Increased expression of YKL-40 mRNA and protein is associated with acute and chronic inflammation, extracellular matrix remodeling, and metastasis (2-10). YKL-40 and its mouse analogue BRP-39 are members of the glycosyl hydrolase family 18 but they lack hydrolytic activity and their physiological role is poorly defined (11). Although little is known about the biological functions of these proteins, recent studies using BRP-39-deficient (BRP-39$^{-/-}$) mice have shed some light on their physiological roles. BRP-39$^{-/-}$ mice had reduced chitin-free antigen-induced Th2

Correspondence and reprint requests to: Dafna Bonneh-Barkay, PhD, 200 Lothrop St. Pittsburgh, PA 15213. Tel: 484-887-0444; Fax: 412-647-5602; dafnabb@yahoo.com.

responses and showed diminished tissue inflammation and fibrosis, increased immune cell apoptosis, and less accumulation of alternatively activated macrophages (12). This suggests that Th2 inflammatory responses are at least partially dependent on BRP-39 expression and that BRP-39 can inhibit death receptor-mediated cell death in immune cells. In contrast, a recent study from the same group showed that BRP-39$^{-/-}$ mice had an increased inflammatory response to hyperoxia that was evident by increased numbers of macrophages and neutrophils in the bronchoalveolar lavage, and premature death (13). This suggests that BRP-39/YKL-40 is involved in regulation of the immune response, but it is not clear whether BRP-39/YKL-40 exacerbates or restricts the inflammatory process.

We found elevated CSF YKL-40 levels in a variety of acute (e.g. viral encephalitis and traumatic brain injury) and chronic (e.g. multiple sclerosis [MS], Alzheimer disease [AD]) neurological conditions, suggesting that YKL-40 might serve as a general surrogate biomarker for neuroinflammation (14, 15). These studies were recently confirmed and extended by others showing that YKL-40 may serve as a prognostic biomarker for preclinical AD and conversion from clinically isolated syndrome to MS (16, 17). We found that YKL-40 transcription and expression are mostly associated with reactive astrocytes and rarely with perivascular macrophages in conditions such as AD, viral encephalitis, the penumbra of brain infarcts and pericontusional areas in an animal model of traumatic brain injury (2, 15). These findings imply that acute inflammation induces YKL-40 expression in astrocytes proximal to the injury site. Our in vitro studies show that YKL-40 transcription is induced in primary astrocytes by inflammatory mediators released from macrophages and is associated with morphological change from homeostatic to reactive phenotype over several days (18).

Reactive astrocytes are a hallmark of neuroinflammatory conditions such as viral encephalitis and MS (14, 19); however, it is unclear whether they contribute or inhibit neuroinflammation. It is well established that astrocytes are able to secrete myriad proinflammatory mediators such as cytokines and chemokines that might influence the inflammatory response (20, 21). On the other hand, Voskuhl et al have shown that reactive scar-forming astrocytes form perivascular barriers that restrict infiltration of leukocytes into the brain parenchyma (22). In order to test the role of BRP-39/YKL-40 in reactive astrocytosis and neuroinflammation, we used a well-characterized model of widespread inflammation in the CNS, experimental autoimmune encephalomyelitis (EAE) in BRP-39$^{-/-}$ mice. Our results imply that BRP-39/YKL-40 expression in reactive astrocytes contributes to the control of neuroinflammation.

MATERIALS AND METHODS

Animals

Mice were rederived by The Jackson Laboratory (Bar Harbor, ME) from BRP-39$^{-/-}$ mice generated in the laboratory of Dr. Jack Elias, as previously described (12). BRP-39$^{-/-}$ mice were subsequently bred onto the C57BL/6 background to create a colony of BRP-39 heterozygous mice from which BRP-39$^{-/-}$ and BRP-39$^{+/+}$ mice were generated. All breeding and genotyping were performed by The Jackson Laboratory. Animal protocols were approved by the University of Pittsburgh Institutional Animal Care and Use Committee.

EAE Induction

Ten-week-old BRP-39$^{-/-}$ (n = 21) and BRP-39$^{+/+}$ littermate control (n = 21) female mice were transferred to The Jackson Laboratory In Vivo Services center in Sacramento, CA. The mice were ear notched for identification and housed in positively ventilated polycarbonate

cages with high-efficiency particulate air (HEPA)-filtered air at a density of 5 mice per cage. Filtered tap water and LabDiets 5K16 were provided ad libitum. Following a 1-week acclimation period, the mice were immunized with 2 subcutaneous flank injections of myelin oligodendrocyte glycoprotein (MOG) peptide (300 μg, amino acids 35-55, purified) emulsified in equal volumes of phosphate buffered saline and complete Freund's adjuvant containing 4 mg/ml of heat-killed *Mycobacterium tuberculosis* on study day 0. Mice received injections of 100 ng of pertussis toxin i.p. on days 0 and 2. The mice were monitored for weight and disease activity that were scored 3 times weekly until day 28. Neurological deficits were graded on a 5-point scale as follows: limp tail or waddling gait = 1; limp tail and ataxia = 2; single limb paresis and ataxia = 2.5; single limb paralysis = 3; single limb paralysis and paresis of second limb = 3.5; full paralysis of two limbs = 4; moribund = 4.5; and death = 5.

Immunohistochemistry

At study days 10 (n = 3), 14 (n = 3) and 28 (n = 6) after MOG immunization (dpi), animals from each group were anesthetized and perfused via the heart with phosphate buffered saline followed by formalin. Brains and spinal cords were post-fixed in formalin. Glial fibrillary acidic protein (GFAP) immunostaining was performed using polyclonal rabbit anti-human GFAP (1:1000; Dako, Carpinteria, CA). Ionized calcium binding adaptor molecule 1 (Iba-1) staining was performed using polyclonal rabbit anti-Iba-1 (1:500; Wako, Richmond, VA). CD3 staining was performed using polyclonal rabbit anti-CD3 (1:500; Dako). All primary antibodies were followed by incubation with appropriate fluorescent or biotin-conjugated secondary antibodies. Fluorescent stains used goat anti-rabbit/mouse Cy3 or goat anti-rabbit/mouse Dylight 488 antibodies (1:200; Jackson Immuno Research Laboratories, West Grove, PA). For immunoperoxidase stains, visualization was performed using VECTASTAIN ABC kit (Vector Laboratories, Burlingame, CA) followed by VECTOR NovaRED Peroxidase Substrate Kit (Vector Laboratories). CD3 staining was counterstained with eosin.

Scoring of Spinal Cord Cell Infiltrates and Demyelination

The presence or absence of inflammatory cell infiltrates was initially established by hematoxylin and eosin staining. Due to the focal nature of the lesions, a semiquantitative scoring was performed. The level of inflammatory cell infiltrate was assigned a score from 0 to 3 as follows: 0 = no inflammatory cell infiltrate; 1 = mild inflammatory cell infiltrate; 2 = moderate inflammatory cell infiltrate; and 3 = severe inflammatory cell infiltrate. Demyelination was assessed by examination of slides stained with Luxol fast blue for 24 hours at 60°C, differentiated in 0.05% lithium carbonate in alcohol, and then counterstained with cresyl violet with acetic acid. Myelination was scored on a scale of 3 to 0: 3 = normal myelination; 2 = mild loss of myelin; 1 = moderate loss of myelin; and 0 = severe loss of myelin.

Whole Slide Tissue Image Analysis

A whole slide tissue image (WSI) for each fluorescent or peroxidase-based immunohistochemical-stained slide was performed as previously described (23, 24). Briefly, WSIs were captured using a Mirax MIDI whole slide high-resolution scanning system (Carl Zeiss MicroImaging, Jena, Germany). Images were generated at a resolution of 0.32 μm/pixel through digitization using an Allied Vision Marlin CCD Camera (Allied Vision Technologies GmbH, Stadtroda, Germany) with a Zeiss Plan-Apopchromat 20X/0.8NA objective. Scanning software provided automated tissue detection, continuous auto-focus during acquisition, and automated alignment of captured fields to create a seamless image. Peroxidase based immunohistochemical-stained slides were scanned using brightfield illumination; immunofluorescent-stained slides were scanned using appropriate fluorescent filters. Image analysis of WSIs was performed with Image Analysis Environment software

(Version 1.8.1.3; Andrew Lesniak Consulting, Pittsburgh, PA) that uses computer assisted color segmentation and builds a range of hue, saturation and value coordinates for the selected fluorescent color points. These values are applied over the entire WSI to create an image that displays intensity values for positive color matches and assigns a 0 to negative color matches. Image Analysis Environment visualization was applied to determine both the percentage of positive color expressing pixels and the percentage of overall tissue area with positive color expression.

In Situ Hybridization

Antisense and sense Brp-39, Cxcl10 or interleukin (Il)1β DNA templates containing the T7/SP6 promoter were generated by PCR using primers from the pUC57 vector (GenScript, Piscataway, NJ) containing full-length Brp-39, Cxcl10 or Il1β cDNA. ^{35}S-labeled RNA probes were generated using MAXIscript in vitro transcription kit (Ambion Inc., Austin, TX). For in situ hybridization (ISH), tissue sections were incubated in hybridization buffer (1X HYB buffer, 0.6M NaCl, 10% dextran, 50 μg/ml tRNA, 0.1M DTT) containing radiolabeled BRP-39 probe (50,000 cpm/μl) at 50°C overnight. The following day, tissue sections were washed and processed for immunofluorescence staining if required. Tissue sections were dipped in emulsion (Eastman Kodak Company, Rochester, NY) and exposed for 10 day at 4°C. The ISH signal was then developed using D19 (Sigma-Aldrich, St. Louis, MO) and fixed by Rapid fix (Sigma-Aldrich). Hybridization of sense probes was not observed on BRP-39$^{+/+}$ tissue.

Microarray Analysis

At 10, 14 and 28 dpi, animals from each group (n = 3) were killed and their brains and spinal cords dissected and flash frozen in liquid N_2. Total RNA was purified from these tissue specimens using the Qiagen RNeasy Midi Kit (Qiagen, Valencia, CA) according to the manufacturer's protocol. The concentration and quality of each RNA sample was evaluated for inclusion in subsequent in vitro transcription assays. Only samples with a spectrophotometric absorption ratio of 260/280 >1.8 (NanoDrop, Wilmington, DE) and a RNA integrity number value of >8.0 via electrophoretic analysis (Agilent Bioanalyzer 2100, Agilent Technologies, Santa Clara, CA) were subjected to in vitro transcription amplification. In vitro transcription was performed using the Ambion MessageAmp Premier Enhanced assay protocol (Ambion, Inc.) starting with 500 ng of purified total RNA. Confirmation of cRNA diversity was obtained using the Bioanalyzer 2100 to generate an electrophoretogram for each in vitro transcription reaction regarding sample yield, integrity, and size diversity against a Universal Human Reference RNA (Stratagene, La Jolla, CA). 15.5 μg of purified, biotin labeled cRNA was fragmented in 30 μL of fragmentation buffer (Ambion MessageAmp Premier RNA Amplification Kit, Ambion, Inc.), followed by resuspension in 270 μL of hybridization buffer (GeneChip Hybridization Control Kit; Wash and Stain Kit; Affymetrix Corp, Santa Clara, CA). Hybridization was performed using 130 μL of the suspended cRNA on Affymetrix Mouse Genome 430A 2.0 arrays (Affymetrix) while subjected to rotation at 60 rpm for 18 hours at 45°C. Washing, staining and scanning of arrays were performed on the Fluidics Station 450 and Scanner 3000 immediately after completion of hybridization. Microarray data was processed using the Expression Console (Affymetrix) with signal intensity calculated by Microarray Suite version 5.0 (MAS 5.0). Differential expression analysis of the intensity data was performed using the Significance Analysis of Microarrays software (version 3.0) with false detection cutoff at $q < 0.05$ (adjusted p value or threshold correction for multiple testing given the actual statistical degrees of freedom) to define median normalized transcripts significantly altered in the experimental paradigm (25). Differentially expressed genes identified at each time-point between BRP-39$^{-/-}$ and BRP-39$^{+/+}$ mice were classified into functional groups and

pathways using Ingenuity Pathways Analysis software (Ingenuity Systems, Redwood City, CA).

Real Time-PCR

Chi3l1, Chi3l3, Cxcl10 and Il1β mRNA quantitation was performed using real-time (RT)-PCR analysis of cDNA. Total RNA was isolated from frozen spinal cords and brains as described in the microarray analysis section. cDNA was synthesized with the RETROscript kit (Life Technologies, Carlsbad, CA) using random decamers. mRNA was evaluated using TaqMan Gene Expression Assays (Life Technologies) for each gene in conjunction with TaqMan Gene Expression Master Mix (Life Technologies). Amplification was assessed on an Applied Biosystems StepONE Real-Time PCR system and analyzed using DataAssist Software (Life Technologies) and the Comparative CT (ddCT) method for each time point. Results were normalized to β2M mRNA expression.

RESULTS

Exacerbation of Clinical EAE in BRP-39$^{-/-}$ Mice

BRP-39$^{-/-}$ mice (n = 21) and their BRP-39$^{+/+}$ littermate controls (n = 21) mice immunized with MOG peptide and pertussis toxin were monitored for disease activity and weight for 28 days. BRP-39$^{-/-}$ mice showed higher clinical EAE scores vs. their BRP-39$^{+/+}$ littermate controls ($P = 0.0058$) (Fig. 1A). BRP-39$^{+/+}$ mice showed an acute monophasic disease (average EAE score of 0.667±0.105) at 10 dpi followed by a recovery period and waning of clinical signs by 28 dpi (average EAE score of 0.111±0.111). In contrast, BRP-39$^{-/-}$ mice displayed an average EAE score of 1.667±0.408 at 15 dpi. BRP-39$^{-/-}$ mice did not show signs of recovery and maintained an elevated EAE clinical score until at least 28 dpi (average EAE score of 1.556±0.294). In addition, BRP-39$^{-/-}$ mice showed significantly lower weights vs. BRP-39$^{+/+}$ littermate controls ($P = 0.0002$) (Fig. 1B).

Exacerbation of Inflammation, Gliosis and Demyelination in BRP-39$^{-/-}$ Mice

At 10 dpi, BRP-39$^{+/+}$ mice (n = 3) did not show the presence of inflammatory cells; 1 out of 3 BRP-39$^{-/-}$ mice showed inflammatory infiltration (Fig. 2A inset). Both wild type and BRP-39$^{-/-}$ mice showed on average equivalent inflammatory infiltrate at 14 dpi (Figure 1B, Supplemental Digital Content 1, http://links.lww.com/NEN/A395) (n = 3 per group). By 28 dpi, none of 6 BRP-39$^{+/+}$ mice showed the presence of inflammatory cells, which correlated with the absence of clinical EAE signs (Figure 1B, Supplemental Digital Content 1, http://links.lww.com/NEN/A395). In contrast, 5 out of 6 BRP-39$^{-/-}$ mice demonstrated mild to severe inflammatory infiltrates at 28 dpi, correlating with the presence of clinical EAE signs (Fig. 2A inset and Figure 1B, Supplemental Digital Content 1, http://links.lww.com/NEN/A395). Immunostaining for CD3 showed abundant T cells in BRP-39$^{-/-}$ mice at 10 dpi vs. BRP-39$^{+/+}$ mice (Fig. 2B). CD3 staining in BRP-39$^{-/-}$ mice remained more abundant than wild type littermates thereafter. WSI analysis confirmed that the percent area of spinal cord tissue sections positive for CD3 immunostaining was lower in most BRP-39$^{+/+}$ mice compared to BRP-39$^{-/-}$ mice (Figure 2B, Supplemental Digital Content 1, http://links.lww.com/NEN/A395). As seen with Iba-1 immunostaining, BRP-39$^{-/-}$ spinal cords also showed abundant macrophages at 14 (data not shown) and 28 dpi compared with BRP-39$^{+/+}$ mice (Fig. 3). In addition to abundant macrophages, BRP-39$^{-/-}$ mice showed substantial astrogliosis as seen with GFAP immunostaining at 28 dpi (Fig. 3). WSI analysis confirmed that the percent area of spinal cord tissue sections positive for Iba-1 and GFAP staining was lower in most BRP-39$^{+/+}$ mice compared with BRP-39$^{-/-}$ mice (Figure 2, Supplemental Digital Content 1, http://links.lww.com/NEN/A395).

Wild type mice with EAE exhibited demyelination during early time points with increased appearance of myelin by 28 dpi (Fig. 2A and Figure 1C, Supplemental Digital Content 1, http://links.lww.com/NEN/A395). BRP-39$^{-/-}$ mice also exhibited a similar degree of early demyelination but at 28 dpi showed significantly less myelin than wild type mice.

BRP-39 Is Induced in Reactive Astrocytes in Lesions During EAE

ISH showed the regional distribution of BRP-39 transcription in BRP-39$^{+/+}$ mice at 10, 14 and 28 dpi (Fig. 4A). BRP-39 mRNA-expressing cells increased at 10 and 14 dpi and began to decline by 28 dpi (Figure 1A, Supplemental Digital Content 1, http://links.lww.com/NEN/A395). Combined BRP-39 ISH and GFAP immunostaining showed that BRP-39 colocalized with GFAP-positive cells in BRP-39$^{+/+}$ mice (Fig. 4B). BRP-39$^{-/-}$ tissue did not show hybridization with the BRP-39 riboprobe (Fig. 4B and Figure 1A, Supplemental Digital Content 1, http://links.lww.com/NEN/A395).

Microarray Analysis of Inflammatory Gene Expression in BRP-39$^{-/-}$ Mice

At 10 days after EAE induction, BRP-39$^{-/-}$ mice had statistically significant increased expression of 17 transcripts and decreased expression of 46 genes. However, by 14 dpi, the response had escalated substantially such that a total of 3064 genes were differentially expressed compared with BRP-39$^{+/+}$ mice (945 increased; 2119 decreased). This transcriptional response was largely sustained 28 dpi with a total of 2767 genes exhibiting significantly different mRNA expression levels (1335 increased; 1432 decreased) vs. BRP-39$^{+/+}$ control littermates. The mRNA expression patterns during EAE in BRP-39$^{-/-}$ and BRP-39$^{+/+}$ mice were subjected to Ingenuity Pathways Analysis using only those transcripts determined to be significantly altered using the Significance Analysis of Microarray software. Table 1 shows a sampling of individual transcripts that were significantly increased in BRP-39$^{-/-}$ mice vs. BRP-39$^{+/+}$ mice at each of the time points. A peak in inflammatory gene expression in BRP-39$^{-/-}$ mice occurred 14 dpi coincident with the elevated clinical disease score. Seven out of 10 molecules overlap between 14 dpi and 28 dpi, thereby supporting the fidelity of the microarray analysis.

Table 2 delineates statistically significant biological networks and their primary functions at each of the time points after EAE induction. At 10 dpi, BRP-39$^{-/-}$ mice exhibited activation of a network that linked IL6 and the BRP-39 protein family member, Chi3l3, which is predominantly associated with cellular movement, hematological system development and cellular growth and proliferation. At 14 dpi, 3 networks were significantly activated, including 2 associated with induction of a prototypical inflammatory response. The first network was composed of 10 genes that are primarily associated with inflammation, cellular movement and hematological system development and function. The second network included processes specifically associated with inflammation, including antigen presentation and cell-cell signaling. The third network is associated with cellular assembly, cellular response to therapeutics, and DNA replication, recombination and repair. At 28 dpi, primary biological networks included molecules involved in cellular assembly, cell morphology and cancer.

Initial validation of the microarray results showed increased transcription of Chi3l3 and Cxcl10 in BRP-39$^{-/-}$ mice by RT-PCR (Fig. 5A) as well as by ISH (Fig. 5B). RT-PCR and ISH for Il1β mRNA, a known inducer of BRP-39 in astrocytes, showed greater levels in BRP-39$^{-/-}$ than in BRP-39$^{+/+}$ mice. All analyses showed that inflammatory gene transcription subsided by 28 dpi in BRP-39$^{+/+}$ mice but remained elevated in BRP-39$^{-/-}$ mice.

DISCUSSION

In this study we used MOG-induced EAE in BRP-39$^{-/-}$ mice to explore the role of BRP-39 in neuroinflammation. We found that BRP-39$^{-/-}$ mice had significantly worse clinical EAE scores and more pronounced neuroinflammation and gliosis. Microarray analysis showed greater induction of inflammatory genes in BRP-39$^{-/-}$ mice, consistent with the clinical and histopathological findings. These results suggest that BRP-39 expression plays a role in restricting inflammatory cell infiltration into the CNS parenchyma and thus modulates neuroinflammation.

The association of BRP-39 with inflammation has been proposed in mouse models of allergic airway inflammation and cigarette smoke-induced inflammation (8, 12, 26). Lee et al were the first to use BRP-39$^{-/-}$ mice in a model of ovalbumin-induced allergic airway inflammation to study the role of mammalian chitinase in asthma. They showed that BRP-39$^{-/-}$ mice had deficiencies in allergen sensitization and Th2 inflammation. BRP-39-deficient mice showed diminished inflammation and fibrosis in the airways together with decreased accumulation of myeloid and plasmacytoid dendritic cells. In addition, increased numbers of apoptotic immune cells (e.g. CD4-positive T cells and macrophages) were detected in the lungs (12). In contrast, a later study from this group showed that BRP-39$^{-/-}$ mice had enhanced inflammatory responses to hyperoxia (13). Prolonged exposure to 100% oxygen caused more severe hyperoxic acute lung injury in BRP-39$^{-/-}$ mice that was characterized by enhanced inflammation, protein leak, oxidation and epithelial cell apoptosis. Interestingly, Nikota et al found that cigarette smoke-induced inflammation was similar in wild type and BRP-39$^{-/-}$ mice with similar total cell, mononuclear cell and neutrophil numbers in the bronchoalveolar lavage (26). As in the hyperoxia model (13), our findings demonstrated a more severe and persistent immune infiltrate in BRP-39$^{-/-}$ vs. BRP-39$^{+/+}$ mice in EAE. Taken together, these results suggest that BRP-39 regulation of inflammation may vary depending upon the specific type of immune activation, cell signaling and tissue involved.

It is intriguing that BRP-39$^{-/-}$ mice showed prolonged retention of CD3-positive cells in both spinal cord and brain compared to wild type mice. This study was limited to a 28-day observation period, which is insufficient to exclude remission in BRP-39$^{-/-}$ mice. It will be important to determine whether retention of T cells in BRP-39$^{-/-}$ mice resolves with longer intervals after immunization or leads to exacerbation of clinical manifestations. Future studies will also need to address how BRP-39/YKL-40 modulates T cell migration, activation and survival during EAE.

As in BRP-39$^{-/-}$ mice, the absence of other astrocyte proteins during EAE leads to exacerbation of clinical disease and alterations in T cell responses. For example, mice lacking astrocyte expression of the cell surface receptor for the IL-6 family of cytokines, gp130, showed increased persistence of activated CD4-positive T cells producing IL-17, interferon (IFN)-γ or tumor necrosis factor (TNF), and activated CD8-positive T cells producing TNF or IFN-γ (27). Alternatively, absence of other proteins might lead to amelioration of disease by limiting recruitment, activation, or survival of T cells after MOG immunization. Osteopontin-deficient mice have a similar appearance of inflammatory cells in the CNS as in wild type mice (28), but show increased cell death in CNS infiltrating T cells by influencing T cell survival through altering expression and activation of transcription factors and pro-apoptotic proteins (29). In view of the complex nature of T cell recruitment, activation/polarization and survival during EAE, BRP-39 might interact directly with T cells or alter T cell dynamics by acting on other CNS cells such as astrocytes or microglia.

Astrocytes are increasingly recognized as regulators of neuroinflammation. Our previous studies showed that YKL-40 (the human homologue of BRP-39) transcription and expression were associated with reactive astrocytes, phenomena that were more pronounced in inflammatory conditions (15). Treating astrocytes with recombinant YKL-40 in vitro led to increased astrocyte cell migration and morphological changes characteristic of reactive gliosis (18). Based on these findings, we believe that YKL-40 expression in astrocytes might function as an autocrine factor that enables astrocytes to limit severity of neuroinflammation.

Recent studies also support the role of astrocytes in restricting inflammatory cell infiltration into the CNS parenchyma (20, 30). Voskuhl et al showed that reactive astrocytes create a barrier-like structure around perivascular inflammatory cells during EAE (22). Transgenic-targeted ablation of reactive astrocytes facilitated infiltration of immune cells into CNS parenchyma. This study confirmed previous studies showing that scar-forming reactive astrocytes create a barrier that restricts infiltration of inflammatory cells from damaged tissue after injury (31-34). Therefore, astrocytes evidently have the capacity to control neuroinflammation during both innate CNS immune responses (e.g. as in TBI or stroke) and adaptive or acquired immune CNS inflammation (e.g. as in EAE). However, it is not clear which astrocyte-derived molecules are responsible for this immune regulation or whether the dense physical barrier that is formed by reactive astrocytes and their secreted extracellular matrix controls trafficking of immune cells. Expression analysis confirmed that BRP-39 transcript levels were absent in BRP-39$^{-/-}$. This finding was consistent with the histologic results and the fact that both inflammatory genes (e.g. Il1β and Cxcl10) and transcripts involved in extracellular matrix remodeling (e.g. Timp1) were significantly increased in BRP-39$^{-/-}$ mice. In addition, mRNA expression of Chi3l3 (Ym1), a member of the chitinase family and a known marker of alternatively activated murine macrophages (35, 36), was greater in BRP-39$^{-/-}$ than in wild type mice at early time points. These changes were consistent with previous studies demonstrating induction of Chi3l3 in microglia in various models of brain injury, such as stab wound, drug-induced seizure, mutant Cu^{2+}/Zn^{2+} superoxide dismutase (mSOD1) ALS mice, and EAE (37-39).

Biological network analysis supported the association of BRP-39 with cellular movement and inflammatory responses, which was compatible with our hypothesis that BRP-39 has a role in the formation of the gliotic scar induced by neuroinflammation. A role for YKL-40 in astrocyte motility was shown by our recent in vitro studies and others demonstrating the ability of YKL-40 to induce astrocyte migration (40). Furthermore, silencing of YKL-40 gene expression in glioblastoma cell lines U373-X3 or U87 reduced their migratory capacity and diminished their invasion ability into Matrigel (40, 41). Future comprehensive microarray studies accompanied with targeted validation will determine the set of genes that are affected by BRP-39 deficiency and will shed light on the cell signaling of BRP-39.

In summary, the aim of this study was to assess whether BRP-39 plays a role in the EAE model. Our findings show that BRP-39 deficiency results in a more severe and persistent disease with enhanced inflammatory cell infiltration and gliosis. Numerous genes were differentially expressed in BRP-39$^{-/-}$ and wild type mice during EAE, including apparent compensation of chitinase family members in the BRP-39-deficient mice. Most differentially expressed genes in BRP-39$^{-/-}$ mice were associated with proinflammatory processes, including cell migration, cell growth, cell proliferation, and antigen presentation. Altered expression of these genes is consistent with the prolonged retention of inflammatory and reactive cells observed in BPR-39$^{-/-}$ mice and dissecting these pathways will shed light on how BRP-39 modulates neuroinflammation. We hypothesize that BRP-39 expression by reactive astrocytes plays a role in the function of the gliotic scar. Future studies are required

to elucidate how mammalian chitinase expression regulates neuroinflammation and whether influencing chitinase expression can modulate neurological outcome.

Supplementary Material

Refer to Web version on PubMed Central for supplementary material.

Acknowledgments

The authors thank Drs. Jack A. Elias and Chun Geun Lee from the Department of Internal Medicine at Yale University School of Medicine for the BRP-39$^{-/-}$ mice. We thank The Jackson Laboratory for performing the EAE studies. We thank Uma Chandran for assistance in analyzing the microarray data. We thank Andrew Lesniak for his expertise in analyzing the Whole Slide Images. We thank Jonette Werley, Arlene Carbone-Wiley, Mark F. Stauffer, and Thomas D. Walko for their valuable technical assistance.

This work was supported in part by a grant from The Pittsburgh Foundation John F. & Nancy A. Emmerling Fund for Medical Research to DB-B. This project used University of Pittsburgh Cancer Institute shared resources that are supported in part by award P30CA047904

REFERENCES

1. Johansen JS. Studies on serum YKL-40 as a biomarker in diseases with inflammation, tissue remodelling, fibroses and cancer. Dan Med Bull. 2006; 53:172–209. [PubMed: 17087877]
2. Bonneh-Barkay D, Zagadailov P, Zou H, et al. YKL-40 expression in traumatic brain injury: an initial analysis. J Neurotrauma. 2010; 27:1215–23. [PubMed: 20486806]
3. Francescone RA, Scully S, Faibish M, et al. Role of YKL-40 in the angiogenesis, radioresistance, and progression of glioblastoma. J Biol Chem. 2011; 286:15332–43. [PubMed: 21385870]
4. Jensen BV, Johansen JS, Price PA. High levels of serum HER-2/neu and YKL-40 independently reflect aggressiveness of metastatic breast cancer. Clin Cancer Res. 2003; 9:4423–34. [PubMed: 14555515]
5. Johansen JS, Hvolris J, Hansen M, et al. Serum YKL-40 levels in healthy children and adults. Comparison with serum and synovial fluid levels of YKL-40 in patients with osteoarthritis or trauma of the knee joint. Br J Rheumatol. 1996; 35:553–9. [PubMed: 8670576]
6. Kaynar MY, Tanriverdi T, Kafadar AM, et al. YKL-40 levels in the cerebrospinal fluid and serum of patients with aneurysmal subarachnoid hemorrhage: preliminary results. J Clin Neurosci. 2005; 12:754–7. [PubMed: 16153848]
7. Koutroubakis IE, Petinaki E, Dimoulios P, et al. Increased serum levels of YKL-40 in patients with inflammatory bowel disease. Int J Colorectal Dis. 2003; 18:254–9. [PubMed: 12673492]
8. Matsuura H, Hartl D, Kang MJ, et al. Role of breast regression protein-39 in the pathogenesis of cigarette smoke-induced inflammation and emphysema. Am J Respir Cell Mol Biol. 2011; 44:777–86. [PubMed: 20656949]
9. Nojgaard C, Host NB, Christensen IJ, et al. Serum levels of YKL-40 increases in patients with acute myocardial infarction. Coron Artery Dis. 2008; 19:257–63. [PubMed: 18480670]
10. Rathcke CN, Kistorp C, Raymond I, et al. Plasma YKL-40 levels are elevated in patients with chronic heart failure. Scand Cardiovasc J. 2010; 44:92–9. [PubMed: 19961288]
11. Hakala BE, White C, Recklies AD. Human cartilage gp-39, a major secretory product of articular chondrocytes and synovial cells, is a mammalian member of a chitinase protein family. J Biol Chem. 1993; 268:25803–10. [PubMed: 8245017]
12. Lee CG, Hartl D, Lee GR, et al. Role of breast regression protein 39 (BRP-39)/chitinase 3-like-1 in Th2 and IL-13-induced tissue responses and apoptosis. J Exp Med. 2009; 206:1149–66. [PubMed: 19414556]
13. Sohn MH, Kang MJ, Matsuura H, et al. The chitinase-like proteins breast regression protein-39 and YKL-40 regulate hyperoxia-induced acute lung injury. Am J Respir Crit Care Med. 2010; 182:918–28. [PubMed: 20558631]

14. Bonneh-Barkay D, Bissel SJ, Wang G, et al. YKL-40, a marker of simian immunodeficiency virus encephalitis, modulates the biological activity of basic fibroblast growth factor. Am J Pathol. 2008; 173:130–43. [PubMed: 18556781]
15. Bonneh-Barkay D, Wang G, Starkey A, et al. In vivo CHI3L1 (YKL-40) expression in astrocytes in acute and chronic neurological diseases. J Neuroinflammation. 2010; 7:34. [PubMed: 20540736]
16. Comabella M, Fernandez M, Martin R, et al. Cerebrospinal fluid chitinase 3-like 1 levels are associated with conversion to multiple sclerosis. Brain. 2010; 133:1082–93. [PubMed: 20237129]
17. Craig-Schapiro R, Perrin RJ, Roe CM, et al. YKL-40: a novel prognostic fluid biomarker for preclinical Alzheimer's disease. Biol Psychiatry. 2010; 68:903–12. [PubMed: 21035623]
18. Bonneh-Barkay D, Bissel SJ, Kofler J, et al. Astrocyte and macrophage regulation of YKL-40 expression and cellular response in neuroinflammation. Brain Pathol. 2012; 22:530–46. [PubMed: 22074331]
19. Adams CW, Poston RN, Buk SJ. Pathology, histochemistry and immunocytochemistry of lesions in acute multiple sclerosis. J Neurol Sci. 1989; 92:291–306. [PubMed: 2809622]
20. Farina C, Aloisi F, Meinl E. Astrocytes are active players in cerebral innate immunity. Trends Immunol. 2007; 28:138–45. [PubMed: 17276138]
21. Nair A, Frederick TJ, Miller SD. Astrocytes in multiple sclerosis: a product of their environment. Cell Mol Life Sci. 2008; 65:2702–20. [PubMed: 18516496]
22. Voskuhl RR, Peterson RS, Song B, et al. Reactive astrocytes form scar-like perivascular barriers to leukocytes during adaptive immune inflammation of the CNS. J Neurosci. 2009; 29:11511–22. [PubMed: 19759299]
23. Isse K, Grama K, Abbott IM, et al. Adding value to liver (and allograft) biopsy evaluation using a combination of multiplex quantum dot immunostaining, high-resolution whole-slide digital imaging, and automated image analysis. Clin Liver Dis. 2010; 14:669–85. [PubMed: 21055689]
24. Isse K, Lesniak A, Grama K, et al. Digital transplantation pathology: combining whole slide imaging, multiplex staining and automated image analysis. Am J Transplant. 2012; 12:27–37. [PubMed: 22053785]
25. Tusher VG, Tibshirani R, Chu G. Significance analysis of microarrays applied to the ionizing radiation response. Proc Natl Acad Sci U S A. 2001; 98:5116–21. [PubMed: 11309499]
26. Nikota JK, Botelho FM, Bauer CM, et al. Differential expression and function of breast regression protein 39 (BRP-39) in murine models of subacute cigarette smoke exposure and allergic airway inflammation. Respir Res. 2011; 12:39. [PubMed: 21473774]
27. Haroon F, Drogemuller K, Handel U, et al. Gp130-dependent astrocytic survival is critical for the control of autoimmune central nervous system inflammation. J Immunol. 2011; 186:6521–31. [PubMed: 21515788]
28. Chabas D, Baranzini SE, Mitchell D, et al. The influence of the proinflammatory cytokine, osteopontin, on autoimmune demyelinating disease. Science. 2001; 294:1731–5. [PubMed: 11721059]
29. Hur EM, Youssef S, Haws ME, et al. Osteopontin-induced relapse and progression of autoimmune brain disease through enhanced survival of activated T cells. Nature Immunology. 2007; 8:74–83. [PubMed: 17143274]
30. John GR, Lee SC, Song X, et al. IL-1-regulated responses in astrocytes: relevance to injury and recovery. Glia. 2005; 49:161–76. [PubMed: 15472994]
31. Bush TG, Puvanachandra N, Horner CH, et al. Leukocyte infiltration, neuronal degeneration, and neurite outgrowth after ablation of scar-forming, reactive astrocytes in adult transgenic mice. Neuron. 1999; 23:297–308. [PubMed: 10399936]
32. Faulkner JR, Herrmann JE, Woo MJ, et al. Reactive astrocytes protect tissue and preserve function after spinal cord injury. J Neurosci. 2004; 24:2143–55. [PubMed: 14999065]
33. Myer DJ, Gurkoff GG, Lee SM, et al. Essential protective roles of reactive astrocytes in traumatic brain injury. Brain. 2006; 129:2761–72. [PubMed: 16825202]
34. Li L, Lundkvist A, Andersson D, et al. Protective role of reactive astrocytes in brain ischemia. J Cereb Blood Flow Metab. 2008; 28:468–81. [PubMed: 17726492]

35. Raes G, De Baetselier P, Noel W, et al. Differential expression of FIZZ1 and Ym1 in alternatively versus classically activated macrophages. J Leukoc Biol. 2002; 71:597–602. [PubMed: 11927645]

36. Mosser DM, Edwards JP. Exploring the full spectrum of macrophage activation. Nat Rev Immunol. 2008; 8:958–69. [PubMed: 19029990]

37. Hung SI, Chang AC, Kato I, et al. Transient expression of Ym1, a heparin-binding lectin, during developmental hematopoiesis and inflammation. J Leukoc Biol. 2002; 72:72–82. [PubMed: 12101265]

38. Beers DR, Henkel JS, Zhao W, et al. Endogenous regulatory T lymphocytes ameliorate amyotrophic lateral sclerosis in mice and correlate with disease progression in patients with amyotrophic lateral sclerosis. Brain. 2011; 134:1293–314. [PubMed: 21596768]

39. Ponomarev ED, Maresz K, Tan Y, et al. CNS-derived interleukin-4 is essential for the regulation of autoimmune inflammation and induces a state of alternative activation in microglial cells. J Neurosci. 2007; 27:10714–21. [PubMed: 17913905]

40. Singh SK, Bhardwaj R, Wilczynska KM, et al. A complex of nuclear factor I-X3 and STAT3 regulates astrocyte and glioma migration through the secreted glycoprotein YKL-40. J Biol Chem. 2011; 286:39893–903. [PubMed: 21953450]

41. Zhang W, Murao K, Zhang X, et al. Resveratrol represses YKL-40 expression in human glioma U87 cells. BMC Cancer. 2010; 10:593. [PubMed: 21029458]

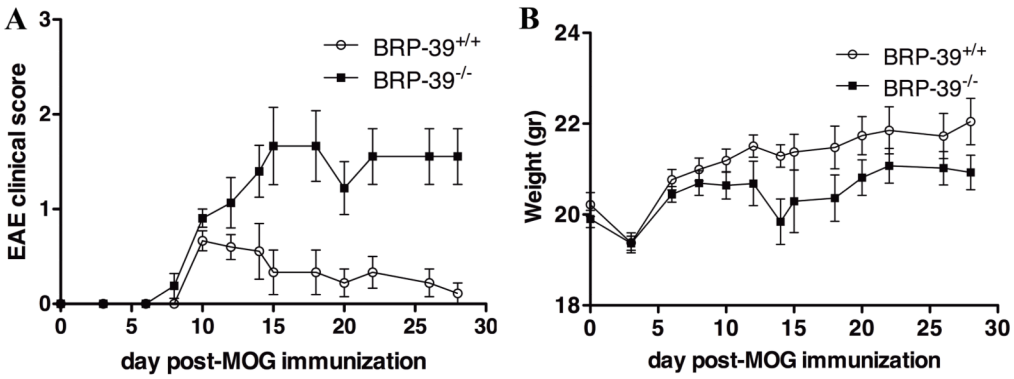

Figure 1.

Exacerbation of experimental autoimmune encephalomyelitis (EAE) clinical score in BRP-39$^{-/-}$ mice. (**A, B**) BRP-39$^{-/-}$ mice (n = 21) and their BRP-39$^{+/+}$ littermate controls (n = 21) were immunized with myelin oligodendrocyte glycoprotein (MOG) peptide and pertussis toxin and monitored for disease activity (**A**) and weight (**B**) for 28 days. BRP-39$^{-/-}$ mice exhibited a more severe and persistent clinical course than BRP-39$^{+/+}$ littermate controls. Data are presented as mean clinical score ± SEM. Wilcoxon match pairs t-test was used to evaluate group differences ($P = 0.0058$ for disease activity; $P = 0.0002$ for weight).

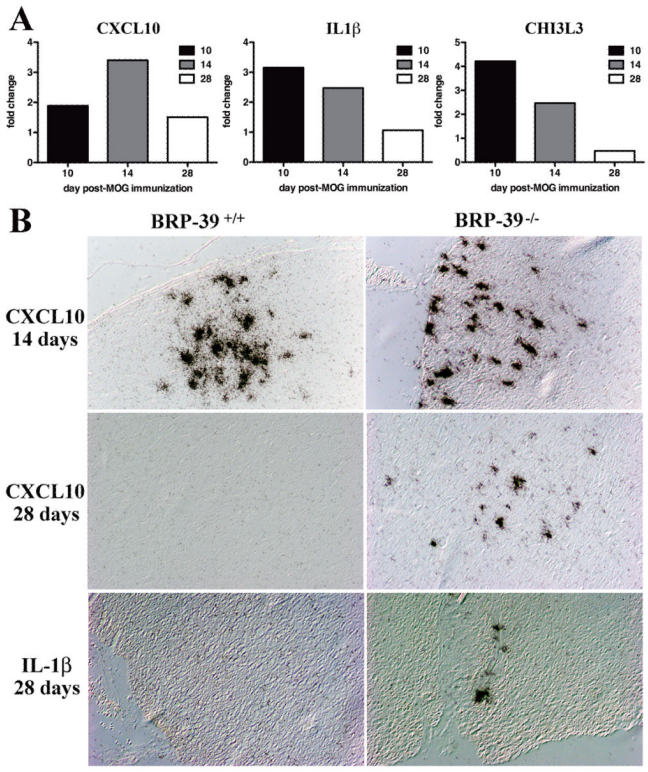

Figure 2.

Increased inflammation in BRP-39$^{-/-}$ mice during EAE. (**A**) Luxol fast blue stain of spinal cord sections at 10, 14 and 28 days post-immunization (dpi) with myelin oligodendrocyte glycoprotein in BRP-39$^{+/+}$ (top row) and BRP-39$^{-/-}$ (bottom row) mice; insets show hematoxylin and eosin staining. At 28 dpi, BRP-39$^{-/-}$ spinal cords showed less myelin staining and more infiltrating inflammatory cells, particularly in submeningeal regions (arrows). Hematoxylin and eosin insets are representative images of equivalently involved lesions of the spinal cords. (**B**) Immunostaining for CD3 in spinal cord sections at 10, 14 and 28 dpi in BRP-39$^{+/+}$ and BRP-39$^{-/-}$ mice. More marked T cell infiltration (arrows) is seen at 14 and 28 dpi in the BRP-39$^{-/-}$ mice.

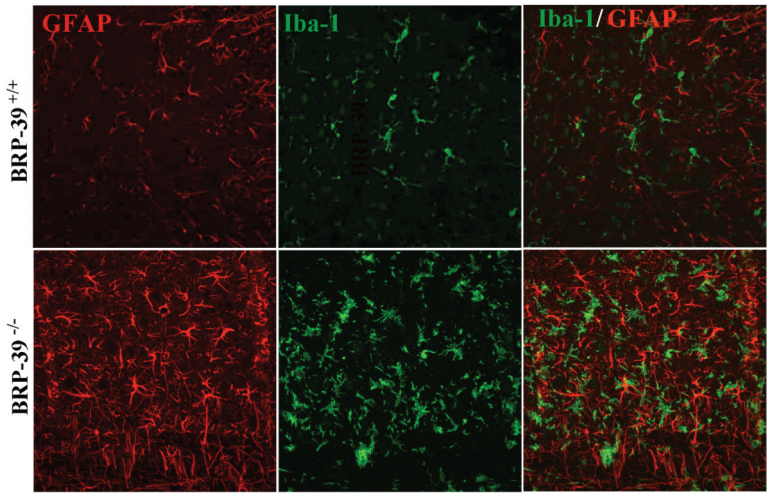

Figure 3.

Gliosis and macrophage activation in BRP-39$^{-/-}$ mice during experimental autoimmune encephalomyelitis. Double-label immunofluorescence for glial fibrillary acidic protein (GFAP) (red) and Iba-1 (green) in spinal cord sections at 28 days post-immunization (dpi) in BRP-39$^{+/+}$ (top row) and BRP-39$^{-/-}$ (bottom row) mice. BRP-39$^{-/-}$ mice show more gliosis and an increased presence of macrophages by 28 dpi vs. BRP-39$^{+/+}$ mice. Representative white matter images were captured from cross sections that best represented the mean of the experimental group.

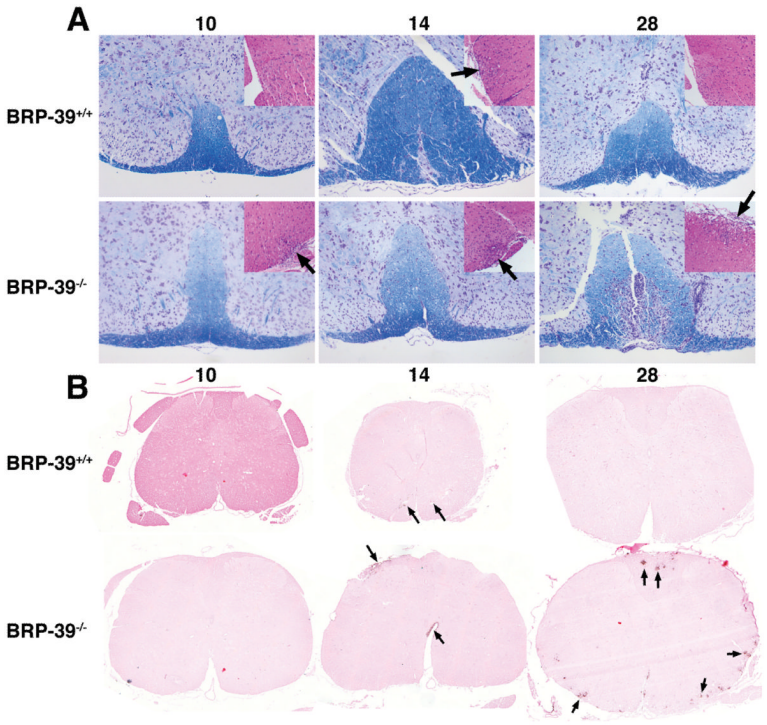

Figure 4.

BRP-39 mRNA transcription in reactive astrocytes during experimental autoimmune encephalomyelitis in BRP-39$^{+/+}$ mice. (**A**) Spinal cord sections were hybridized with a ^{35}S-labeled RNA probe for BRP-39. BRP-39 transcription is evident at 10 days post-immunization (dpi), reaching a peak at 14 dpi, and subsiding by 28 dpi. (**B**) Spinal cord sections were hybridized with a ^{35}S-labeled RNA probe for BRP-39 (black grains) followed by glial fibrillary acidic protein (GFAP) immunostaining (green). BRP-39 mRNA co-localized with GFAP green fluorescent signal in BRP-39$^{+/+}$ spinal cords (top row). Spinal cords from BRP-39$^{-/-}$ mice showed no significant hybridization in gliotic regions.

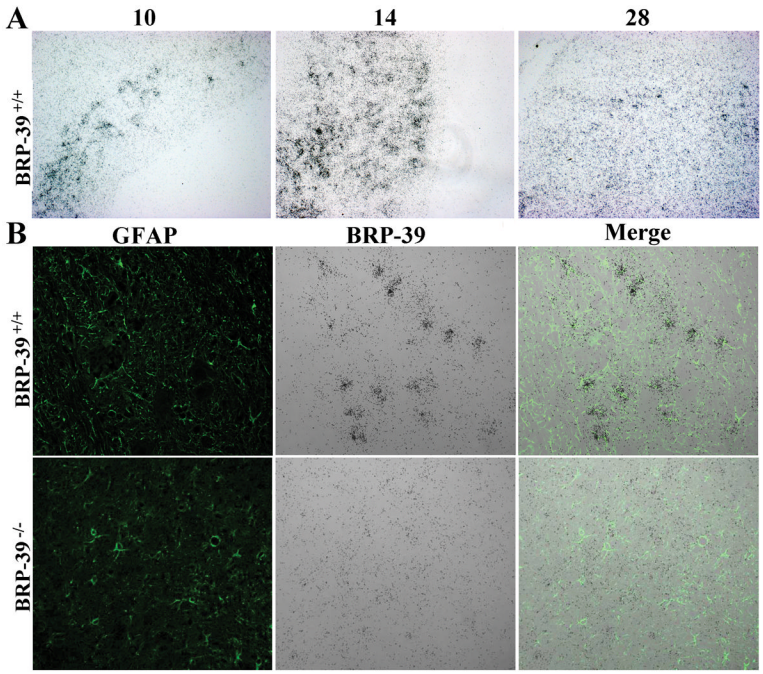

Figure 5.

Increased Chi3l3, Cxcl10 and Il1β transcription in BRP-39$^{-/-}$ mice compared with BRP-39$^{+/+}$ mice. (**A**) Total RNA from spinal cord and brain was assessed for Cxcl10, Il1β, or Chi3l3 mRNA expression using RT-PCR. The fold change between each transcript from BRP-39$^{-/-}$ and BRP-39$^{+/+}$ mice was determined by the Comparative Ct method for each time point. CNS tissue from BRP-39$^{-/-}$ mice showed greater expression of proinflammatory molecules Cxcl10 and Il1β in addition to increased expression of the chitinase Chi3l3. (**B**) In situ hybridization (ISH) for Il1β and Cxcl10 showed increased expression in BRP-39$^{-/-}$ spinal cords (right column) compared with BRP-39$^{+/+}$ spinal cords (left column) at 28 days post-immunization (dpi). Micrographs illustrate representative expression of Cxcl10 at 14 and 28 dpi and Il1β at 28 dpi. Chi3l3, Chitinase 3-like 3; Cxcl10, Chemokine (C-X-C motif) ligand 10; IL-1β, interleukin-1β; MOG, myelin oligodendrocyte glycoprotein.

Table 1

Genes Increased in the CNS of BRP-39$^{-/-}$ vs. BRP-39$^{+/+}$ Mice During EAE

Day 10		Day 14		Day 28	
Gene symbol	Fold change*	Gene symbol	Fold change	Gene symbol	Fold change
Chi3l3	↑4.945	Cxcl10	↑7.92	Timp1	↑3.386
S100a9	↑3.547	Cxcl9	↑7.563	Clec7a	↑3.013
S100a8	↑3.182	Clec7a	↑6.596	H2-Ab1	↑2.466
Camp	↑2.655	Chi3l3	↑6.049	H2-Aa	↑2.413
		H2-Aa	↑5.575	Fcgr2b	↑2.269
		Bat2	↑5.229	Lgals3	↑2.255
		Lgals3	↑5.109	C1qB	↑2.144
		Fcgr2b	↑5.051	Ccl2	↑2.143
		H2-Ab1	↑4.541	Cxcl9	↑2.133
		Lcn2	↑4.533	SerpinA3n	↑2.105
		Timp1	↑4.421		

Abbreviations: Chi3l3, Chitinase 3-like 3); S100a9, S100 calcium binding protein A9; S100a8, S100 calcium binding protein A8; Camp, Cathelicidin antimicrobial peptide; Cxcl10, chemokine (C-X-C motif) ligand 10; Cxcl9, chemokine (C-X-C motif) ligand 9; Clec7a, C-type lectin domain family 7, member a; H2-Aa (histocompatibility 2, class II antigen Aa); Bat2 (HLA-B associated transcript 2); Lgals3 (Lectin, galactose-binding, soluble 3); Fcgr2b (Fc receptor, IgG, low affinity IIb); H2-Ab1 (histocompatibility 2, class II, antigen A, beta 1); Lcn2 (Lipocalin 2); Timp1 (Tissue inhibitor of metalloproteinase 1); C1qB (Complement component 1, q subcomponent, beta polypeptide); Ccl2 (Chemokine (C-C motif) ligand 2, SerpinA3n (serine (or cysteine) pepitidase inhibitor, clade A, member 3N).

*Fold change between BRP-39$^{-/-}$ and BRP-39$^{+/+}$ mice.

Table 2

Ingenuity Analysis of Biological Networks and Functions of Genes Differentially Increased in BRP-39$^{-/-}$ CNS Compared with BRP-39$^{+/+}$ CNS During EAE

DPI	Network number for each dpi	Differentially increased molecules in network*	Biological functions of network
10	1	↑Chi3l3/Chi3l4, Il6	Cellular movement, Hematological system development and function, Cellular growth and proliferation
14	1	Atf4, birc2, ↑Casp4, ↑Cd68, ↑Chi3l3/Chi3l4, Csf1, Cxcl1, Cxcl2, ↑Emr1, Fas, ↑Icam1, Il6, Il12b, ↑Il1b, Lif, Nfkb1, Nos2, Plau, Ptgs2, ↑SerpinA3n, ↑Socs3, Sod2, ↑Stat1, ↑Tlr2, TNF	Cellular movement, Inflammatory response, Hematological system development and function
14	2	Bcar1, ↑Hck	Antigen presentation, Cell-to-cell signaling and interaction, Inflammatory response
14	3	Dhx9, Prkdc, Xrcc5, Xrcc6, ↑Zic2	Cellular assembly and organization, DNA replication, recombination and repair, Cellular response to therapeutics
28	1	Il1B, ↑SerpinA3n	Cellular assembly and organization, Endocrine system disorders, Gastrointestinal disease
28	2	Rara, ↑Vim	Cancer, Cardiovascular system development and function, cell morphology

Abbreviations: Chi3l3, Chitinase 3-like 3; S100a9, S100 calcium binding protein A9; S100a8, S100 calcium binding protein A8; Camp, Cathelicidin antimicrobial peptide; Cxcl10, Chemokine (C-X-C motif) ligand 10; Cxcl9, Chemokine (C-X-C motif) ligand 9; Clec7a, C-type lectin domain family 7, member a; Emr1, EGF-like module-containing mucin-like hormone receptorlike 1; H2-Aa, histocompatibility 2, class II antigen A, alpha; Bat2, HLA-B associated transcript 2; IL6, interleukin-6; Lgals3, Lectin, galactose-binding, soluble 3; Fcgr2b, Fc receptor, IgG, low affinity IIb; Icam1, intercellular adhesion molecule-1; H2-Ab1, histocompatibility 2, class II, antigen A, beta 1; Lcn2, Lipocalin 2; Timp1, Tissue inhibitor of metalloproteinase 1; C1qB, Complement component 1, q subcomponent, beta polypeptide; Ccl2, Chemokine (C-C motif) ligand 2, SerpinA3n, (serine, or cysteine) pepitidase inhibitor, clade A, member 3N); Socs, suppressor of cytokine signaling 3; Vim, vimentin

*Underlined molecules were differentially increased in BRP-39$^{-/-}$ CNS vs. BRP-39$^{+/+}$ CNS. DPI, days post-immunization.